

Preparation of TiO₂ nanoparticles by the sol–gel method under different pH conditions and modeling of photocatalytic activity by artificial neural network

Mohammad A. Behnajady · Hamed Eskandarloo

Received: 28 March 2013 / Accepted: 19 June 2013 / Published online: 6 July 2013
© Springer Science+Business Media Dordrecht 2013

Abstract In this study, TiO₂ nanoparticles were prepared by the sol–gel method under different pH conditions and the structural properties of TiO₂ nanoparticles were obtained by X-ray diffraction and transmission electron microscopy. The photocatalytic activity of TiO₂ nanoparticles was studied in the removal of C.I. Acid Red 27 (AR27) under UV light. The desired gelation pH for photocatalytic removal of AR27 was obtained at pH 5. At this pH, the predominant crystal phase of TiO₂ is anatase and its crystallite size is smaller than at other gelation pHs. The artificial neural network (ANN) technique was applied to model and predict the photocatalytic activity of TiO₂ nanoparticles prepared at the desired gelation pH. Four effective operational parameters were inserted as the inputs of the network and reaction rate constants (k_{ap}) were introduced as the outputs of the network. The results showed that the predicted data from the designed ANN model are in good agreement with the experimental data with a correlation coefficient (R^2) of 0.9852 and mean square error of 0.00242. The designed ANN provides a reliable method for modeling the photocatalytic activity of TiO₂ nanoparticles under different operational conditions. Furthermore, the relative importance of each operational parameter was calculated based on the connection weights of the ANN model. The initial dosage of TiO₂ nanoparticles was the most significant parameter in the photocatalytic removal of AR27, followed by the UV-light intensity and initial AR27 concentration.

Keywords Heterogeneous photocatalysis · TiO₂ nanoparticles · Gelation pH · C.I. Acid Red 27 · Artificial neural network · Operational parameters

M. A. Behnajady (✉)

Department of Chemistry, Faculty of Science, Tabriz Branch, Islamic Azad University, Tabriz, Islamic Republic of Iran
e-mail: behnajady@gmail.com; behnajady@iaut.ac.ir

H. Eskandarloo

School of Chemistry, College of Science, University of Tehran, Tehran, Islamic Republic of Iran

Introduction

Wastewaters generated from textile industries constitute one of the largest groups of organic compounds which are a serious threat to the environment [1, 2]. In recent years, there has been a growing interest in the development of new processes for water treatment, since the traditional physical treatment processes only transfer the contaminants from the wastewater to other media [3]. The heterogeneous photocatalysis process, based on a combination of UV irradiation and a semiconductor, represents one of AOPs that provide an interesting route to the destruction of many organic substances to CO_2 , H_2O , and corresponding mineral acids [4]. When a semiconductor absorbs a photon with energy greater than or equal to the band gap energy, valence band electrons are promoted to the conduction band leaving a hole behind. These electron–hole pairs can either recombine or interact separately with other molecules [5]. Reactions between adsorbed water, hydroxyl anions, and oxygen molecules or other substances with electron and hole pairs produced at the semiconductor surface under UV irradiation produce hydroxyl radicals. The hydroxyl radical is a powerful oxidizing agent and attacks organic compounds [6].

Titanium dioxide exists in three crystalline phases: anatase, rutile, and brookite [7, 8]. The predominant commercial phase of TiO_2 is anatase which has been widely studied because of its high activity in photocatalytic applications. Anatase with a tetragonal crystal structure and a band gap of 3.23 eV has been used in photocatalytic processes [8, 9]. In comparison with the other forms of titania, the rutile form is stable. Rutile has a crystal structure similar to that of anatase, with the exception that the octahedral shares four edges instead of four corners. Rutile with a band gap of 3.0 eV has been used as a whitening agent [10, 11]. Brookite has an orthorhombic crystal structure and spontaneously transforms to rutile around 750 °C [8]. TiO_2 is extensively used as an active component for photocatalytic reactions. It is nontoxic, stable within a wide range of pH, inexpensive, and, due to a fast electron transfer to molecular oxygen, is found to be very efficient for photocatalytic removal of pollutants [12, 13]. There are many variables that affect the photocatalytic activity of TiO_2 , such as particle size, crystal structure, and the preparation method of particles. Crystal structure and particle size are considered as important factors that determine photoactivity [14, 15].

In recent years, many researchers have applied artificial neural networks (ANNs) for simulations in various fields. For example, Frontisti et al. applied the ANN technique to modeling of the photocatalytic (UV-A/ TiO_2) degradation of 17 α -ethynylestradiol (EE2) in different operational conditions [TiO_2 and EE2 concentration, reaction time, organic content and conductivity of the water matrix (DOC)] by TiO_2 -P25 nanoparticles. They have reported that the ANN can be a reliable method of semiempirical models in wastewater treatment. By using the ANN model, they have calculated the relative significance of the operational parameters on the value of EE2 photocatalytic degradation, and the following order for variables effects was achieved by the ANN model: reaction time \approx matrix conductivity > TiO_2 concentration > estrogen concentration \approx matrix DOC [16]. Khatamian et al. employed ANN to predict the performance of photocatalytic degradation of 4-nitrophenol (4-NP) using ZnO nanoparticles supported on zeolites. They have reported that the ANN model was

successful in predicting the performance of photocatalytic degradation of 4-NP in aqueous solution. Furthermore, the sensitivity analysis showed that the following order for variables effects was predicted by the ANN model: pH (52.39 %) > Time (35.87 %) > initial 4-NP concentration (11.74 %) [17].

In this study, TiO₂ nanoparticles were prepared by the sol–gel method under different gelation pH conditions and the effect of the gelation pH was studied on the phase structure, crystallite size, and photocatalytic activity. Photocatalytic removal of C.I. Acid Red 27 (AR27) was chosen as a probe reaction to measure the photocatalytic activity of TiO₂ nanoparticles. The effects of some operational parameters (such as TiO₂ dosage, initial AR27 concentration, initial pH of solution, and UV-light intensity) on the photocatalytic removal of AR27 were studied and modeled by using a multilayer feed-forward neural network model. Furthermore, the relative importance of each operational parameter was calculated based on the connection weights of the ANN model.

Experimental

Materials

The following commercial reagents were used: titanium tetraisopropoxide (TTIP) [Ti(OC₃H₇)₄; Merck], sodium hydroxide (NaOH), nitric acid (HNO₃) and methanol (MeOH) with absolute grade. AR27 which is a monoazo anionic dye was obtained from Merck and used without further purification. Figure 1 displays the structure of this dye. All other reagents were of analytical grade. Solutions were prepared by dissolving the required quantity of the AR27 and the prepared photocatalyst in double-distilled water.

Preparation of TiO₂ nanoparticles

TiO₂ nanoparticles were prepared from TTIP as a titanium precursor, in methanol and distilled water. Initially, TTIP was slowly dissolved in the methanol with molar

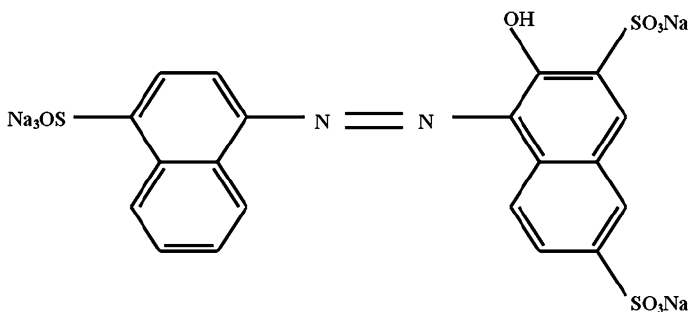


Fig. 1 Molecular structure of AR27

ratios 1:1. Then, the obtained titanium solution was sonicated in an ultrasonic bath (Elma, T460/H, 35 kHz, 170 W). The hydrolysis of the alkoxide was then performed by adding water dropwise into a flask containing (precursor/solvent) mixture under reflux and magnetic stirring for 3 h at 80 °C. The hydrolysis process was carried out at different pH values, adjusted by the addition of NaOH or HNO₃. The obtained sol was dried at 80 °C and finally calcined in air at 450 °C during 3 h. Phase composition and crystallite size of TiO₂ nanoparticles were analyzed by X-ray diffraction (XRD) measurements which were carried out at room temperature by using a Siemens XRD D5000 with Cu K α radiation ($\lambda = 0.15478$ nm). The size of the synthesized TiO₂ nanoparticles was obtained by a transmission electron microscopy (TEM) instrument (Philips CM-10 HT-100 keV). The specific surface area and pore-size distribution of the synthesized TiO₂ nanoparticles were measured by nitrogen adsorption–desorption at 77 K using the BET method (Belsorp mini II instrument).

Photodegradation procedure

Removal of the azo-dye AR27 from aqueous solution was used as a model reaction to evaluate the photocatalytic activity of the prepared TiO₂ nanoparticles. Photocatalytic removal of AR27 was carried out in a batch quartz photoreactor of 100 mL volume with a low-pressure mercury UV-C lamp (15 W, Philips, Netherlands) emitting around 254 nm, in the parallel array, which was placed in front of the quartz tube reactor. The light intensity in the center of the quartz photoreactor was measured using a Lux-UV-IR meter (Leybold, Germany). In each run, 40 mg of TiO₂ nanoparticles was added to 100 mL of the solution and fed into the quartz tube reactor. At given irradiation time intervals, the samples (5 mL) were taken out and then analyzed by a UV–Vis spectrophotometer (Pharmacia Biotech Ultrospec 2000) at 522 nm.

Results and discussion

Characterization of TiO₂ nanoparticles

The identification of the phase of the TiO₂ nanoparticles and the grain size was done with XRD. Figure 2 depicts the XRD patterns of TiO₂ nanoparticles prepared by the sol–gel method under different pH conditions.

The average crystallite size (D in nm) of TiO₂ nanoparticles was determined from XRD patterns according to the Scherrer's equation [18];

$$D = \frac{k\lambda}{\beta \cos \theta} \quad (1)$$

where k is a constant equal to 0.89, λ , the X-ray wavelength equal to 0.154056 nm, β , the full width at half maximum intensity (FWHM), and θ , the half diffraction angle. The phase structure of a sample can be calculated from the integrated intensities of anatase (I_A) and rutile (I_R) peaks using the following equation [19];

$$\text{Rutile phase \%} = \frac{100}{1 + 0.8 \left(\frac{I_A}{I_R} \right)} \quad (2)$$

Crystallite size and the amount of each phase of TiO₂ nanoparticles as a function of gelation pH are presented in Table 1. In the obtained nanopowders, a mixture of anatase and rutile phases with crystallite size between 12–23 nm was identified. The percent of the anatase phase is at its highest value at pH 5. Also, the crystallite size of TiO₂ nanoparticles in this pH is smaller than other gelation pHs. The crystallite size of the TiO₂ nanoparticles is same at pH 3 and pH 10, but the amount of the anatase phase at pH 3 is higher than at pH 10. The results show that synthesis of TiO₂ nanoparticles with different crystalline phases is possible only with changing the gelation pH in the synthesis period.

Transmission electron microscopy analysis allows the direct deduction of mean particle size. The TEM image of the TiO₂ nanoparticles prepared at gelation pH 5 with smaller crystallite size than other samples is shown in Fig. 3. The average particle size of the TiO₂ nanoparticles was found to be <15 nm, which is in agreement with the crystallite size calculated from the XRD pattern.

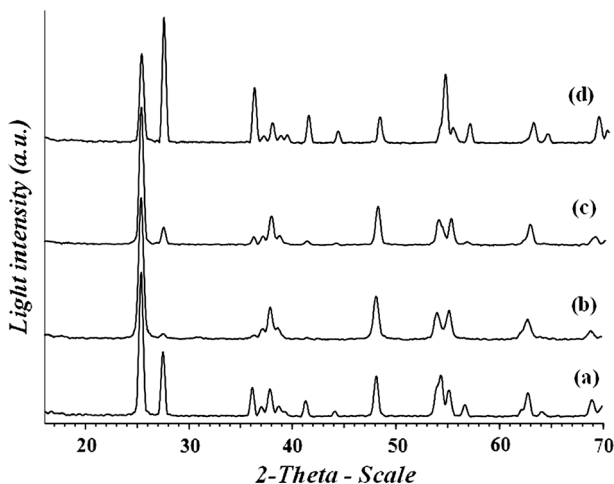


Fig. 2 X-ray diffraction for TiO₂ nanoparticles prepared by the sol-gel method at different gelation pH: a pH 3; b pH 5; c pH 7; d pH 10

Table 1 Crystallite size and phase structure of TiO₂ nanoparticles prepared at different gelation pH

Gelation pH	Amount of each phase %	Crystallite size (nm)
3	A: 65, R: 35	D _A : 19, D _R : 22
5	A: 95, R: 5	D _A : 15, D _R : 12
7	A: 86, R: 14	D _A : 18, D _R : 19
10	A: 37, R: 63	D _A : 19, D _R : 22

A Anatase, R rutile, D_A average crystallite size of anatase phase, D_R average crystallite size of rutile phase

Figure 4 displays the nitrogen adsorption–desorption isotherm of TiO_2 nanoparticles prepared at gelation pH 5. At high relative pressures from 0.55 to 0.85, the isotherms exhibit hysteresis loops of H2 type indicating the existence of an ink-bottle-type pores structure with narrow necks and wide bodies [20, 21]. The BET surface area and total pore volume for TiO_2 nanoparticles prepared at gelation pH 5 were $99.71 \text{ m}^2 \text{ g}^{-1}$ and $0.2169 \text{ cm}^3 \text{ g}^{-1}$, respectively. The average pore size obtained by the BJH model (Fig. 4 inset) was 8.7 nm, suggesting the presence of mesoporous structure.

Fig. 3 TEM image of TiO_2 nanoparticles prepared at gelation pH 5

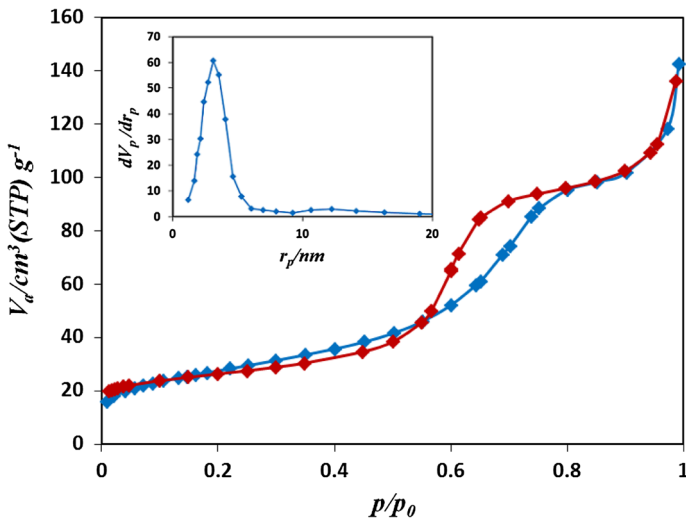
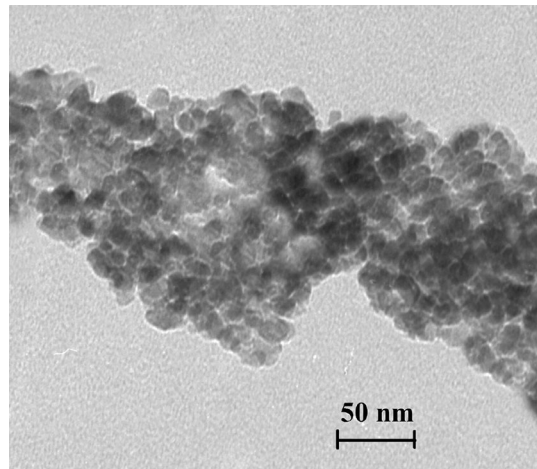


Fig. 4 The N_2 adsorption–desorption isotherm and BJH pore size distribution curve (*inset*) of TiO_2 nanoparticles prepared at gelation pH 5

Photocatalytic activity

The adsorption of AR27 onto TiO₂ nanoparticles was negligible at the initial pH of 5. Interactions between AR27 molecules with anionic character and TiO₂ nanoparticles will be favored at very acidic pHs. The semi-logarithmic graph of the concentration of AR27 in the presence of TiO₂ nanoparticles prepared at different gelation pH versus UV light irradiation time yields straight lines, which confirm the pseudo-first-order kinetics for decolorization of AR27 in this process. Figure 5 shows the variation of the pseudo-first-order reaction rate constant (k_{ap}) for removal of AR27 with TiO₂ nanoparticles prepared at different gelation pH. As can be seen from this Figure, the maximum photocatalytic activity of the TiO₂ nanoparticles was obtained at gelation pH 5. This can be the result of a higher percentage of the anatase phase and also the smaller size of the nanoparticles at this gelation pH. The anatase phase of TiO₂ has higher photocatalytic activity in comparison with the rutile phase. Because the anatase phase has a wider band gap (~ 3.2 eV) than that of TiO₂ rutile phase (~ 3.0 eV), the electron–hole separation in anatase phase therefore occurs better than in the rutile phase [22–24]. Barati et al. studied the influence of sol pH on the particle size of TiO₂ nanostructures. They have reported that when the pH increases from 4.5 to 7, the particle size of the TiO₂ thin film increases. Transformation from Ti(OH)₄ to anatase TiO₂ and nucleation of anatase are assumed to be inhibited by excessive adsorption of hydroxyl ions to TiO₂ clusters [25]. Zhang et al. prepared TiO₂ nanoparticles using the reverse micelle method under acidic conditions. It was found that the concentration of the acid has a major role in the formation of rutile phase, and higher acid concentration (2.5 M) is better for rutile crystallization. Their product was a mixture of anatase and rutile when the concentration of acid was 2 M [26]. Wei et al. studied the effect of pH in the range of 7–11 on phase content and particle size of TiO₂ catalysts. They reported that the presence of a high concentration of hydroxyl ions is more suitable for the formation of the rutile phase [27]. The results in Fig. 5 and Table 1 show that the photocatalytic activity of TiO₂ nanoparticles prepared at different gelation pH decreases with decreasing the percentage of the anatase phase so that the photocatalytic activity of the TiO₂ nanoparticles prepared at gelation pH 10 is very low in comparison with other gelation pHs.

Artificial neural network (ANN) modeling

Artificial neural networks are a quite appropriate modeling technique for their ability of learning, simulation, and prediction of experimental data. A multilayered perceptron (MLP) neural net has one input layer of the neuron (independent variables), a number of hidden layers, and the output layer (dependent variables). The number of input and output neurons is fixed by the nature of the problem. The hidden layers act like feature detectors, and there can be more than one hidden layer [28, 29].

In this work, Matlab v.2011a mathematical software was used for ANN calculations and a three-layered back-propagation algorithm with tangent sigmoid transfer function (tansig) at hidden layer, and a linear transfer function (purelin) at

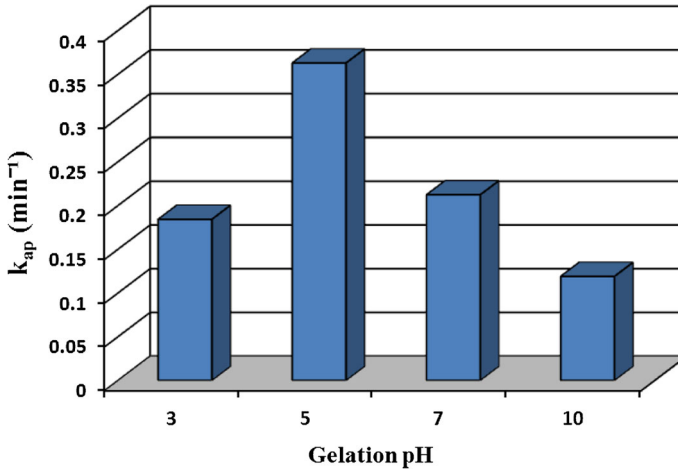


Fig. 5 Effect of gelation pH on photocatalytic activity of TiO_2 nanoparticles prepared by the sol-gel method

Table 2 The ranges of input and output variables

Variable	Range of the parameter value
Input layer	
TiO_2 dosage (g L^{-1})	0.01–0.05
Initial AR27 concentration (mg L^{-1})	10–50
Initial pH	5–9
UV light intensity (W m^{-2})	15.5–56.5
Output layer	
k_{ap} (min^{-1})	0.058–0.6529

output layer, was designed. The input variables of the network were the TiO_2 dosage, initial AR27 concentration, initial pH of solution, and UV-light intensity, and the corresponding reaction rate constant (k_{ap}) was used as an output of the network. The ranges of operational parameters are given in Table 2.

The ANN model was used from experimental datasets in different conditions for test training. The experimental datasets were split into training (one-half), validation (one-fourth) and test (one-fourth) subsets. All inputs and target data were scaled within a specified range. Therefore, all data (X_i) were scaled (x_i) into the 0.2–0.8 range through the following equation (3) [30, 31]:

$$x_i = 0.2 + \frac{0.6(X_i - X_{\min})}{(X_{\max} - X_{\min})} \quad (3)$$

where X_{\min} and X_{\max} refer to the lowest and highest value of the input variable X_i , respectively.

The numbers of neurons in the hidden layer are affecting on the performance of an ANN model. In this study, to determine the optimum number of hidden nodes,

different numbers of neurons tested in the range from 1 to 12, in the hidden layer. Each topology was repeated three times to avoid random correlation due to the random initialization of the weights. Figure 6 shows the relationship between the mean square error (MSE) and the number of neurons in the hidden layer. As can be seen, the lowest MSE was obtained in about 8 neurons; therefore, 8 neurons were selected for the best performance of the neural network model. Figure 7 shows the schematic illustration of the optimized ANN structure.

Figure 8 shows a comparison between experimental and predicted k_{ap} values for the test set by using the neural network model. The plot in this Figure has a correlation coefficient (R^2) of 0.9852. From this plot, it can be seen that the results obtained from the model are in good agreement with the experimental data, and that the model can accurately predict reaction rate constants at different operational conditions.

For the test of the designed ANN model performance in the modeling of other organic pollutants, we employed photocatalytic removal of C.I Acid Red 88 (AR88) by TiO₂-P25 nanoparticles. The results indicated that the predicted data from the designed ANN for photocatalytic removal of AR88 are in good agreement with the experimental data with a correlation coefficient (R^2) of 0.9566. Therefore, we conclude that the designed ANN is a reliable model for modeling of the photocatalytic removal of different organic pollutants under different operational conditions.

Optimization and modeling of operational parameters

To optimize the operational parameters in the photocatalytic removal of AR27 by using TiO₂ nanoparticles prepared by the sol-gel method at gelation pH 5, four operational parameters, TiO₂ dosage, initial AR27 concentration, initial pH of solution, and UV-light intensity, were studied.

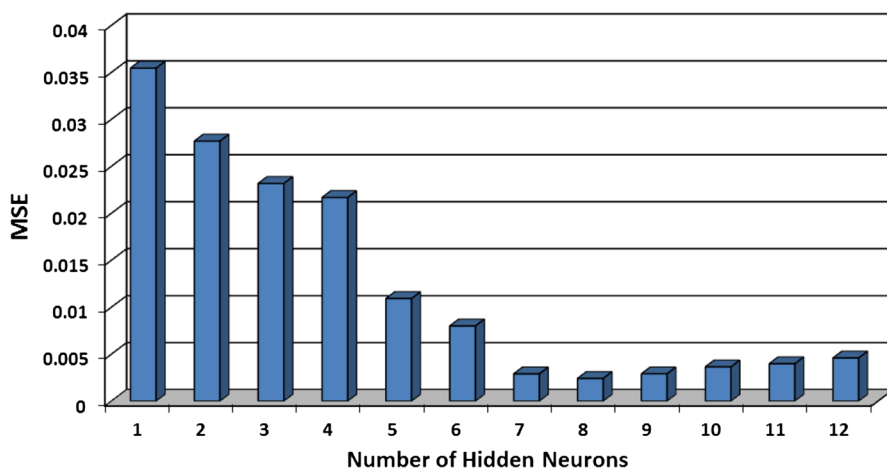


Fig. 6 Effect of the number of neurons in the hidden layer on the performance of the neural network

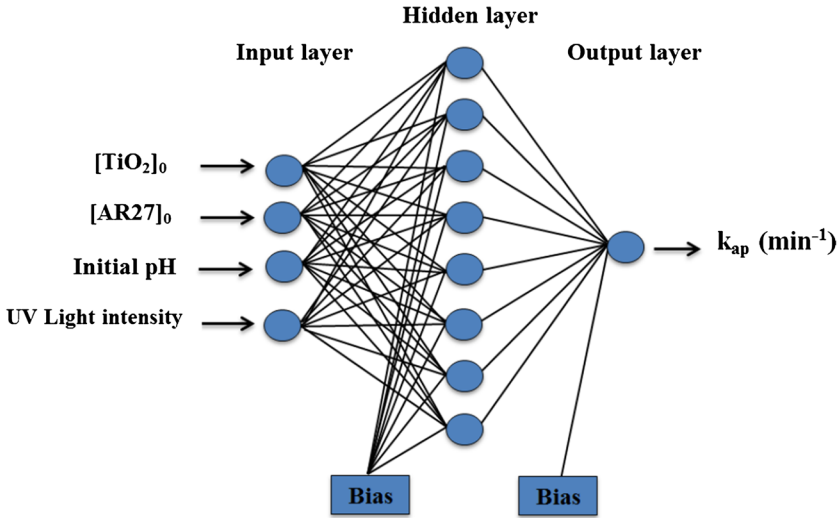


Fig. 7 Schematic illustration of the optimized ANN structure

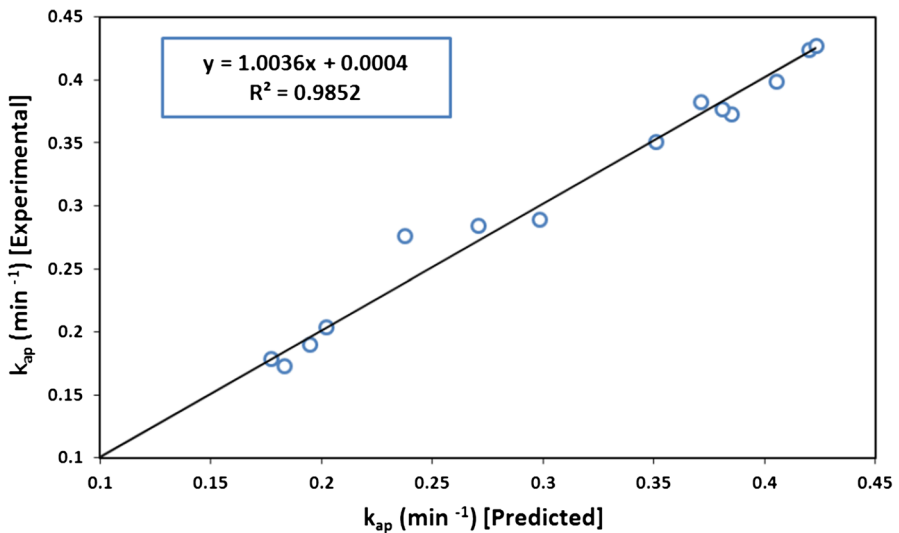


Fig. 8 Comparison between predicted and experimental k_{ap} values for the test set

Effect of TiO_2 dosage

The influence of TiO_2 loading on the photocatalytic removal rate of AR27 was studied using TiO_2 dosages in the range of 0.1–0.5 $g L^{-1}$. Figure 9 shows the variation of the removal rate for AR27 as a function of catalyst dosage. It can be seen from this Figure that the increase in the TiO_2 dosage until 0.4 $g L^{-1}$ improves the removal rate of AR27. This could be the result of increasing of

available adsorption and catalytic sites on the TiO₂ surface which are responsible for photocatalytic activity [14]. Improvement of the removal rate is not obvious above 0.4 g L⁻¹ because, at high catalyst loading, the turbidity of the solution and scattering effect increases which causes a decrease in UV light penetration into the solution [32]. Figure 9 shows that the neural network model correctly predicts k_{ap} of the AR27 removal by TiO₂ nanoparticles as a function of the catalyst dosage.

Effect of initial AR27 concentration

It is important from an application point of view to study the dependence of the removal rate on the initial concentration of the pollutant. The effect of the initial concentration of AR27 on the photocatalytic removal rate was studied over the concentration range of 10–50 mg L⁻¹ of AR27 (Fig. 10). The results show that the removal rate decreases as the initial AR27 concentration increases. This can be due to the following reasons:

- With increasing of the pollutant concentration, more and more organic substances and intermediates are adsorbed on the surface of TiO₂ nanoparticles, and therefore the generation of active species such as hydroxyl radicals will be reduced [33, 34].
- With increasing of the pollutant concentration, the solution becomes impermeable to UV radiation because the molar extinction coefficient of the AR27 at 254 nm (the wavelength of UV lamp) is very high, so the photons get intercepted before they can reach the catalyst surface [14]. Figure 10 shows a good agreement between the k_{ap} of AR27 removal calculated from the ANN model and the experimental results as a function of the initial concentration of the dye.

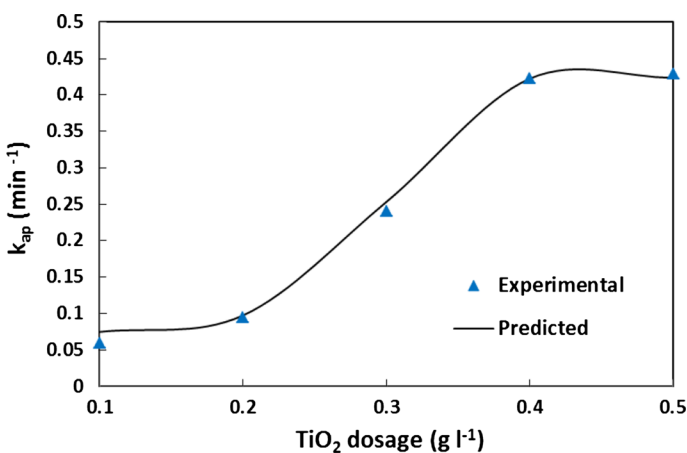


Fig. 9 Influence of TiO₂ dosage on the removal rate of AR27. [AR27]₀ = 20 mg L⁻¹, I₀ = 56.5 W m⁻², pH of solution = 5

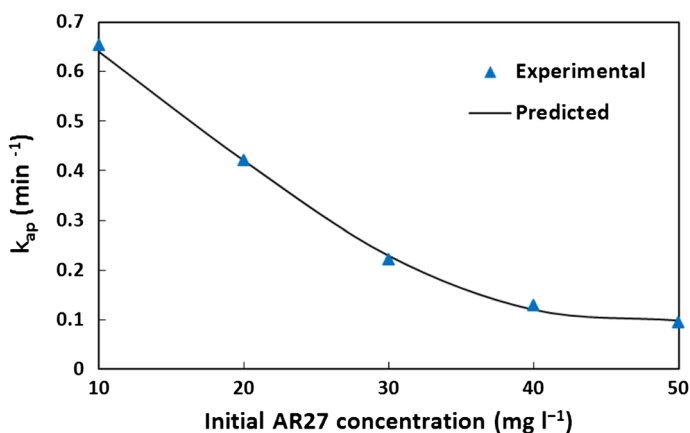


Fig. 10 Influence of initial AR27 concentration on the removal rate of AR27. $[\text{TiO}_2]_0 = 0.4 \text{ g L}^{-1}$, $I_0 = 56.5 \text{ W m}^{-2}$, pH of solution = 5

Effect of initial pH of solution

An important parameter which affects the rate of photocatalytic reactions is the pH of the solution, because it dictates the surface charge properties of the photocatalyst and the size of aggregates that it forms. The removal of the pollutant was studied at different initial pH of solution values in the range 5–9. The pH of the reaction mixture was adjusted by adding a dilute aqueous solution of HCl or NaOH. The removal rate of AR27 as a function of the initial pH of solution is shown in Fig. 11. The results show that the removal efficiency of AR27 was carried out effectively at an initial pH 5, while increasing the pH causes a decrease of the removal rate.

The pH of the solution can affect the surface charge of the photocatalyst and also shift the potential of some redox reactions. Thus, it affects the adsorption of organic solutes on the catalyst surface, and consequently its reactivity to active species formed at the surface. The amphoteric behavior of most semiconductor oxides influences the surface charge of the photocatalyst: the photocatalyst surface is positively charged in acidic media, whereas it is negatively charged under alkaline conditions [35, 36]. Under acidic media, adsorption of AR27 molecules effectively occur on the TiO_2 surface because AR27 molecules are anionic and the catalyst surface as the result of proton adsorption is positively charged. The increase in the photocatalytic removal rate in acidic pH may be due to the high adsorption of AR27 molecules on the TiO_2 surface. Figure 11 shows that the neural network model correctly predicts the k_{ap} of the AR27 removal by the TiO_2 nanoparticles as a function of the initial pH of the solution.

Effect of light intensity

The influence of UV-light intensity on the removal rate of AR27 has been monitored by increasing the UV-light intensity from 15.5 to 56.5 W m^{-2} . Figure 12 shows the

effect of light intensity on the removal rate of AR27 with TiO₂ nanoparticles prepared by the sol–gel method. It appears from Fig. 12 that, by increasing the light intensity from 15.5 to 56.5 W m⁻², the removal rate increases, because the UV-light irradiation generates the photons needed for the electron transfer from the valence band to the conduction band of a semiconductor photocatalyst. When the light intensity is low, the electron–hole separation competes with recombination and decreases the formation of hydroxyl radicals. The rate of decolorization increases when more radiation falls on the catalyst surface and hence more hydroxyl radicals are produced [6, 32, 37]. Figure 12 shows good agreement between the k_{ap} of AR27 removal calculated from the ANN model and the experimental results as a function of UV-light intensity.

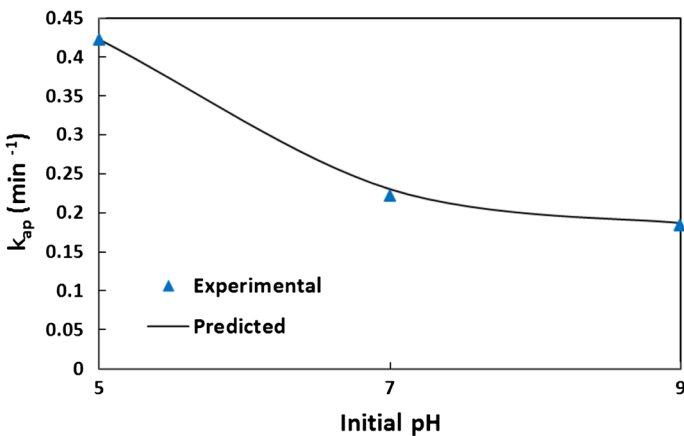


Fig. 11 Influence of initial pH of the solution on the removal rate of AR27. [TiO₂]₀ = 0.4 g L⁻¹, [AR27]₀ = 20 mg L⁻¹, I₀ = 56.5 W m⁻²

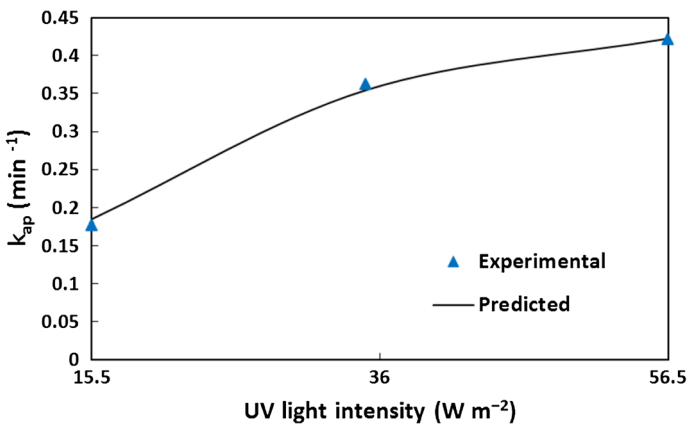


Fig. 12 Influence of UV light intensity on the removal rate of AR27. [TiO₂]₀ = 0.4 g L⁻¹, [AR27]₀ = 20 mg L⁻¹, pH of solution = 5

Table 3 Weight matrix: weights between input and hidden layers (W_1) and weights between hidden and output layers (W_2)

Neuron	W_1							W_2	
	Input variable							Output	
	[TiO ₂] ₀	[AR27] ₀	Initial pH	UV light intensity	Bias	Neuron	k_{ap} (min ⁻¹)		
1	-0.8130	1.3584	-1.1645	1.2740	2.3676	1	-0.2324		
2	-1.2261	-1.8623	-0.4234	1.1351	1.4307	2	0.9090		
3	1.1968	1.8567	-0.6725	1.0472	-0.7864	3	0.7298		
4	-1.4969	1.2459	-1.2841	-0.3746	0.4273	4	-0.2495		
5	-1.7892	-1.3283	0.8230	-0.2195	-0.0855	5	-0.1601		
6	1.7602	-0.9517	0.4003	-1.1823	0.7527	6	-0.3141		
7	0.4048	0.6549	1.8290	0.8540	1.8221	7	-0.6973		
8	0.4794	-1.6712	-1.5555	-0.3419	2.3213	8	0.4704		
						Bias	-0.0602		

ANN model sensitivity analysis

Table 3 shows the weights produced by the ANN model used in this study. The relative importance of the influence of each input variable on the output variable can be obtained through the neural weights matrix [38].

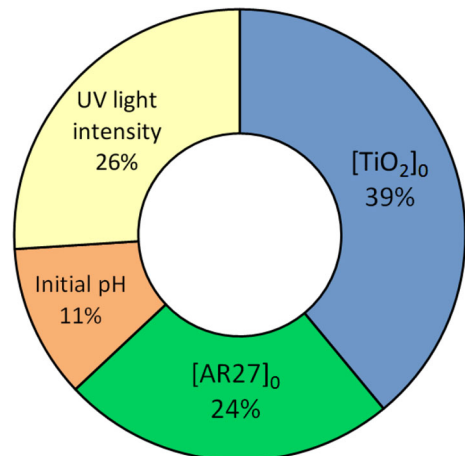
For every input operational parameter, the percentage change in the output, as a result of the change in the input variable, was calculated using the following equation (4) [31, 38]:

$$I_j = \frac{\sum_{m=1}^{m=N_h} \left(\left(\frac{|W_{jm}^{ih}|}{\sum_{k=1}^{N_i} |W_{km}^{ih}|} \right) \times |W_{mn}^{ho}| \right)}{\sum_{k=1}^{k=N_i} \left\{ \sum_{m=1}^{m=N_h} \left(\frac{|W_{km}^{ih}|}{\sum_{k=1}^{N_i} |W_{km}^{ih}|} \right) \times |W_{mn}^{ho}| \right\}} \quad (4)$$

where I_j is the relative importance of the j th input variable on the output variable, N_i and N_h are the numbers of input and hidden neurons, respectively, W 's are connection weights, the superscripts 'i', 'h', and 'o' refer to input, hidden, and output layers, respectively, and subscripts 'k', 'm', and 'n' refer to input, hidden, and output neurons, respectively.

Figure 13 represents a comparison between the effects of the four input operational parameters as calculated by equation (4) on the photocatalytic removal of AR27. As can be seen, the dosage of TiO₂ nanoparticles with a relative importance of 39 % has a larger effect on the photocatalytic removal of AR27, followed by the UV-light intensity and the initial AR27 concentration, with relative importance of 26 and 24 %, respectively, while the initial pH of solution, with a relative importance of 11 %, was determined as the parameter with weak influence on the photocatalytic removal of AR27.

Fig. 13 Relative importance (%) of the input operational parameters on the k_{ap} values of the AR27 removal



Conclusions

We have successfully prepared TiO₂ nanoparticles with crystallite size between 12 and 23 nm and different phase structures by the sol–gel method. TiO₂ with mainly anatase phase (95 % anatase and 5 % rutile) can be prepared by adjusting the gelation pH to a value of 5. The test of photocatalytic activity indicates that the desired gelation pH for high photocatalytic activity is pH 5. In this study, the effect of some operational parameters on the photocatalytic removal of AR27 was modeled by the ANN technique. A three-layered back-propagation neural network with tangent sigmoid transfer function (tansig) at the hidden layer with 8 neurons was designed to predict the removal of AR27 under different operational conditions. The performance of prepared TiO₂ nanoparticles in the dye removal was successfully simulated by using neural network modeling, and a good agreement was obtained between the predicted results from the ANN model and the experimental results, with a correlation coefficient (R^2) of 0.9852 and MSE 0.00242. The sensitivity analysis showed that the initial dosage of the prepared TiO₂ nanoparticles has a larger effect on the photocatalytic removal of AR27, while the initial pH of solution has the lowest effect on the photocatalytic removal of AR27.

Acknowledgments The authors would like to thank the financial support of Tabriz Branch, Islamic Azad University and the Iranian Nanotechnology Initiative Council.

References

1. M.A. Khosa, S.S. Shah, J. Disper. Sci. Technol. **32**, 1002 (2011)
2. J. Guo, Y. Du, Y. Lan, J. Mao, J. Hazard. Mater. **186**, 2083 (2011)
3. O.J. Hao, H. Kim, P.C. Chiang, Crit. Rev. Environ. Sci. Technol. **30**, 449 (2000)
4. M.A. Behnajady, H. Eskandarloo, N. Modirshahla, M. Shokri, Photochem. Photobiol. **87**, 11002 (2011)
5. M.A. Behnajady, H. Eskandarloo, N. Modirshahla, M. Shokri, Dig. J. Nanomater. Biostruct. **6**, 1887 (2011)
6. N. Daneshvar, M. Rabbani, N. Modirshahla, M.A. Behnajady, J. Photochem. Photobiol. A **168**, 39 (2004)
7. G.L. Chiarello, A.D. Paola, L. Palmisano, E. Selli, Photochem. Photobiol. Sci. **10**, 355 (2011)
8. M.A. Behnajady, H. Eskandarloo, N. Modirshahla, M. Shokri, Desalination **278**, 10 (2011)
9. Z. Wang, S.K. Saxena, V. Pischedda, H.P. Liermann, C.S. Zha, J. Phys. Condens. Matter **13**, 8317 (2001)
10. W.-J. Yin, S. Chen, J.-H. Yang, X.-G. Gong, Y. Yan, S.-H. Wei, Appl. Phys. Lett. **96**, 221901 (2010)
11. N.R. Mathews, M.A. Corte Jacome, E.R. Morales, J.A. Toledo Antonio, Phys. Status Solidi C **6**, S219 (2009)
12. K. Naeem, F. Ouyang, Physica B **405**, 221 (2010)
13. I. Řehoř, V. Kubíček, J. Kotek, P. Hermann, J. Száková, I. Lukeš, Eur. J. Inorg. Chem. **2011**, 1981 (2011)
14. M.A. Behnajady, N. Modirshahla, M. Shokri, H. Elham, A. Zeininezhad, J. Environ. Sci. Health A **43**, 460 (2008)
15. H.-D. Jang, H. Chang, K. Cho, S.J. Kim, J.H. Park, J.W. Choi, K. Okuyama, Ultramicroscopy **108**, 1241 (2008)
16. Z. Frontistis, V.M. Daskalaki, E. Hapeshi, C. Drosoua, D. Fatta Kassinos, N.P. Xekoukoulotakis, D. Mantzavinos, J. Photochem. Photobiol. A **240**, 33 (2012)
17. M. Khatamian, B. Divband, A. Jodaiei, Mater. Chem. Phys. **134**, 31 (2012)
18. A.L. Patterson, Phys. Rev. **56**, 978 (1939)

19. R.A. Spurr, H. Myers, *Anal. Chem.* **29**, 760 (1957)
20. F. Dumeignil, K. Sato, M. Imamura, N. Matsubayashi, E. Payen, H. Shimada, *Appl. Catal. A* **241**, 319 (2003)
21. K.S.W. Sing, D.H. Everett, R.A.W. Haul, L. Moscou, R.A. Pierotti, J. Rouquerol, T. Siemieniewska, *Pure Appl. Chem.* **57**, 603 (1985)
22. S.S. Hong, C.S. Ju, C.G. Lim, B.H. Ahn, K.T. Lim, G.D. Lee, *J. Ind. Eng. Chem.* **7**, 99 (2001)
23. J. Lu, P. Zhang, A. Li, F. Su, T. Wang, Y. Liu, *J. Gong. Chem. Commun.* **49**, 5817 (2013)
24. A.R. Gandhe, S.P. Naik, J.B. Fernandes, *Microporous Mesoporous Mater.* **87**, 103 (2005)
25. N. Barati, M.A. Faghihi Sani, H. Ghasemi, Z. Sadeghian, S.M.M. Mirhoseini, *Appl. Surf. Sci.* **255**, 8328 (2009)
26. D. Zhang, L. Qi, J. Ma, H. Cheng, *J. Mater. Chem.* **12**, 3677 (2002)
27. Q. Wei, R. Cheng Jun, G. Mao Chu, H. Yun Ze, C. Yao Qiang, *Acta Phys. Chim. Sin.* **27**, 1487 (2011)
28. V.K. Pareek, M.P. Brungs, A.A. Adesina, R. Sharma, *J. Photochem. Photobiol. A* **149**, 139 (2002)
29. D. Salari, N. Daneshvar, F. Aghazadeh, A.R. Khataee, *J. Hazard. Mater.* **125**, 205 (2005)
30. M.B. Kasiri, H. Aleboyeh, A. Aleboyeh, *Environ. Sci. Technol.* **42**, 7970 (2008)
31. A. Aleboyeh, M.B. Kasiri, M.E. Olya, H. Aleboyeh, *Dyes Pigm.* **77**, 288 (2008)
32. M.A. Behnajady, N. Modirshahla, R. Hamzavi, *J. Hazard. Mater.* **133**, 2226 (2006)
33. C.G. Silva, J.L. Faria, *J. Mol. Catal. A* **305**, 147 (2009)
34. M.A. Behnajady, N. Modirshahla, N. Daneshvar, M. Rabbani, *Chem. Eng. J.* **127**, 167 (2007)
35. V. Mirkhani, S. Tangestaninejad, M. Moghadam, M.H. Habibi, A. Rostami Vartooni, *J. Iran. Chem. Soc.* **6**, 578 (2009)
36. M. Uğurlu, M.H. Karaoğlu, *Fresenius Environ. Bull.* **19**, 2883 (2010)
37. A.A. Khodja, T. Sehili, J. Pilichowski, P. Boulez, *J. Photochem. Photobiol. A* **141**, 231 (2001)
38. G.D. Garson, *AI Expert* **6**, 47 (1991)